IBRACON Structures and Materials Journal
Revista IBRACON de Estruturas e Materiais
ISSN 1983-4195 ismj.org

ORIGINAL ARTICLE

Prediction of the ultimate capacity of reinforced concrete elements using nonlinear analysis methodologies

Predição da capacidade última de elementos em concreto armado usando metodologias de análises não linear

Ingrid Rocio Irreño Palomo[a]
Juan de Jesus Martínez[a]
Carlos Alberto Benedetty[a]
Luiz Carlos de Almeida[a]
Leandro Mouta Trautwein[a]
Pablo Augusto Krahl[b]

[a]Universidade Estadual de Campinas – UNICAMP, Faculdade de Engenharia Civil, Departamento de Estruturas, Campinas, SP, Brasil
[b]Universidade Presbiteriana Mackenzie – UPM, Faculdade de Engenharia Civil, Departamento de Estruturas, Campinas, SP, Brasil

Received 27 October 2022
Revised 01 May 2023
Accepted 20 May 2023
Corrected 27 March 2024

Abstract: This work aims to investigate the ultimate capacity of reinforced concrete elements in terms of cracking and stiffness loss. Nonlinear finite element analysis (NLFEA) was performed in the ATENA software and compared with a proposed numerical simulation of nonlinear static analysis (NLSA), where material cracking is evaluated based on the loss of tangent stiffness of the elements. The analysis was applied to a low-rise reinforced concrete frame with constant axial loads in the columns, and monotonic lateral load applied at the top beam level. Both methodologies showed good agreement regarding the capacity curve and crack patterns, and the numerical simulation NLSA allowed the identification of the sequence of elements' stiffness loss. The results indicated a substantial similarity between the numerical simulation NLFEA and NLSA and the experimental test, indicating a high potential in predicting the nonlinear behavior of reinforced concrete.

Keywords: reinforced concrete, frames, nonlinear analysis, cracking.

Resumo: Este trabalho tem como objetivo investigar a capacidade última de elementos em concreto armado em termos de fissuração e perda de rigidez. Uma análise não linear via método dos elementos finitos (MEF) foi realizada no programa ATENA e comparada com uma simulação numérica de análise estática não linear (AENL), onde a fissuração do material é avaliada com base na perda de rigidez tangente dos elementos. As análises foram aplicadas a um pórtico em concreto armado com cargas axiais constantes nos pilares, e carga lateral monotônica aplicada na viga superior. Ambas as metodologias mostraram boa concordância em relação à curva de capacidade e panorama de fissuração, e a simulação numérica AENL permitiu identificar a sequência de perda de rigidez dos elementos. Os resultados indicaram grande semelhança entre a simulação numérica FEM e AENL e ensaio experimental, indicando um alto potencial para prever o comportamento não linear do concreto armado.

Palavras-chave: concreto armado, pórticos, análise não-linear, fissuração.

How to cite: I. R. I. Palomo, J. J. Martínez, C. A. Benedetty, L. C. Almeida, L. M. Trautwein, and P. A. Krahl, "Prediction of the ultimate capacity of reinforced concrete elements using nonlinear analysis methodologies," *Rev. IBRACON Estrut. Mater.*, vol. 17, no. 2, e17210, 2024, https://doi.org/10.1590/S1983-41952024000200010

Corresponding author: Ingrid Rocio Irreño Palomo. E-mail: ingridpal2393@gmail.com
Financial support: The authors greatly appreciate the financial support provided by the Brazilian National Council for Scientific and Technological Development (CNPq) (Grant 141517/2021-2).
Conflict of interest: Nothing to declare.
Data Availability: data-sharing is not applicable to this article as no new data were created or analyzed in this study.
This document has an erratum: https://doi.org/10.1590/S1983-41952024000200011

1 INTRODUCTION

The prediction of the behavior and ultimate capacity of reinforced concrete (RC) structures has shown significant advances in the last decades due to the evolution of technology that allows the use of computers with a higher processing capacity to analyze nonlinear phenomena, such as plastification and fracture. However, these phenomena can be complex to be reproduced in numerical simulation of quasi-brittle materials such as concrete. Depending on the type of problems analyzed, models can have many degrees of freedom, reducing the processing capacity and simulation feasibility. Commercial software can be used for the nonlinear analysis of reinforced concrete structures, which implement the Finite Element Method (FEM). Some examples are: ABAQUS [1], ANSYS [2], ATENA [3], and DIANA [4].

FEM is especially suitable for studying the cracking behavior and plastic hinges, which are considered the leading sources of nonlinearity in structures. Based on this approach, the Extended Finite Element Method (X-FEM) proposed by Belytschko and Black [5], can simulate the cracking and localized deformations of specimens with simple and complex geometries, being an advantage of the independence of the discretization of the mesh. However, a major drawback is the necessity to generate a variable number of degrees of freedom in each node [6], [7]. The Finite Elements Method with Embedded Strong Discontinuities (ED-FEM) also allows the modeling of the failure zones discretely without the re-meshing through a static condensation of the global system of equations with the same number of nodal displacements (or degrees of freedom) as the initial problem (without the discontinuity).

The method of zero-thickness interface elements initially proposed by Goodman et al. [8] is capable of representing the cracking behavior of quasi-brittle materials (e.g., concrete), where the interface elements are connected with the continuum elements through constitutive laws that are governed by normal and tangential components of the stress and their relative displacements [8]–[10]. The main advantage of it is the capacity to solve problems that involve material interfaces or discontinuities. However, Dhadse et al. [11] describe the implementation of a thin-layer interface as a drawback. Authors such as Manzoli et al. [12], [13] presented a new technique to model interfaces through solid finite elements (three-node triangular finite element), e.g., elements with a very high aspect ratio, where the smallest dimension corresponds to the thickness of the interface. Due to its high aspect ratio, this method does not depend on mesh size in the interface region.

Regarding numerical simulations with Nonlinear Finite Element Analysis (NLFEA), Alfarah et al. [14] developed a methodology applied to damage models in the ABAQUS software based on the formulations of Lubliner et al. [15] and Lee and Fenves [16] to analyze reinforced concrete frames with monotonic behavior. This methodology enabled the establishment of the tension–compression damage of the material in function of the strains. Additionally, Guner [17] restructured and verified the analytical algorithm of the VecTor5 program, used for the nonlinear analysis of frames based on MCFT [18], to capture the shear mechanisms and bending effects in the elements. Besides enhancing the original monotonic analysis, this algorithm also allows the analysis of frames subject to cyclic load, dynamic load, impact load, blast, etc. The author applied the algorithm with and without geometrical nonlinearity in the structure, with the latter overestimating the ultimate capacity of the frame.

In nonlinear problems, the load can be applied by a force or incremental displacement steps that cause variation in the stiffness of the structure, requiring the reassembly of the stiffness matrices and higher computational cost [19]. However, dividing the structure into undamaged (elastic) and damaged (nonlinear) substructures helps decrease computational effort. In the first case, the matrix formulation is developed before the nonlinear analysis, while in the second case, the stiffness is variable for each load increment and numerical iteration [19], [20].

Caglar et al. [21] stated that concrete cracking affects the behavior of reinforced concrete elements by reducing their flexural and shear stiffness. Thus, the linear elastic analysis of RC elements without considering the cracking effect does not represent the real behavior. Furthermore, Chan et al. [22] concluded that the cracking effect in a reinforced concrete frame is generally considered through the reduced inertia moments of the elements. The same authors proposed a general probability-based effective stiffness model that determines the relationship between flexural stiffness reductions and moments caused by the load applied. The methodology was developed through iterative algorithms, which can also be used for elements subjected to various types of loads. The advantage of this method was the ability to estimate the lateral deflection and stiffness of tall reinforced concrete frames under service loads. They obtained good results when compared with experimental data tests and observed that the flexural stiffness reduction caused by the cracking significantly influences the load-deformation curve of the structures.

In addition, Ng et al. [19] developed a nonlinear multilevel analysis method for RC frames, which divided the elements into subelements to evaluate stiffness degradation and strength deterioration. In this process, the stiffness of subelements is estimated from the moment-curvature relations, where the curvature is assessed based on the transverse displacements and section rotations. In this work, the authors only considered the boundary degrees of freedom associated with the boundary nodes, obtaining an ultimate load capacity 7% lower than the experimental value.

Subsequently, Guner and Vecchio [23] studied the analytical method developed by the same authors [24], which analyzed the nonlinear behavior of reinforced concrete frame structures composed of beams, columns, and shear walls under monotonic and pushover loading. The method uses a nonlinear sectional analysis within a stiffness-based linear-elastic frame analysis algorithm through an unbalanced force approach, which allows capturing shear mechanisms through modeling based on the Disturbed Stress Field Model (DSFM). The authors observed excellent convergence and numerical stability characteristics in the results with little demanding computational time (around 1 and 6 minutes for beams and frames, respectively).

Recently, Hippola et al. [25] developed a new force-base line element formulation based on the formulation proposed by Rajapakse et al. [26] to predict the axial-force-moment interaction and, therefore, the response of reinforced concrete frames and walls. The relationship between element nodal forces and section forces is known, causing a reduction of the number of degrees of freedom in the numerical model compared to displacement-based formulations. Additionally, the authors employed the tangent stiffness matrices to improve convergence speed and the constitutive relationship of the DSFM instead of the Modified Compression Field Theory (MCFT). The results allowed identifying shear critical members in large frame structures and estimating the distribution of internal forces, crack patterns, capacity load, and failure modes. However, the methodology was unable to predict the strength degradation displacements for the shear-compression and the diagonal-tension failure modes.

As a contribution to the study of the nonlinearity behavior of the concrete, this work proposes to combine a Nonlinear Finite Element Analysis (NLFEA) with a new Nonlinear Static Analysis (NLSA) to assess the ultimate capacity, cracking sequence and stiffness loss of a two-way, one-level reinforced concrete frame structure, which was part of an experimental campaign developed by Vecchio and Emara [27], in order to verify the influence of shear strains on structure design and behavior. For this, a numerical simulation of NLFEA was carried out in the ATENA software, and a numerical simulation involving an optimized NLSA with stiffness degradation. One of the best advantages of the new optimized numerical simulation NLSA is that elements discretization does not increase the system degree of freedom, simplifying the calculation of the displacements and forces of the structure.

2 EXPERIMENTAL TEST

Vecchio and Emara [27] conducted an experimental study at the University of Toronto addressing low-rise reinforced concrete frame to investigate the shear effects in the ultimate capacity and strains of the structure. The frame had two levels of 1800 mm and 1600 mm and a 3100 mm span. Beams had a 300×400 mm transversal section, whereas columns had a 400×300 mm section and were subjected to a strongly reinforced base of 5700×800×400 mm (Figure 1).

B1 and B2 refer to first and second-level beams, while C1-C3 and C2-C4 are the left and right columns of the frame, respectively. Beams and columns were longitudinally reinforced by eight bars of 20 mm diameter, four bars in the upper face, and four bars in the bottom face. Transversal reinforcement was performed by 10 mm stirrups positioned at a 125 mm spacing. The reinforced concrete base includes 21 bars of 20 mm diameter and stirrups placed at each 250 mm. A 700 kN vertical load was applied to each column, representing the upper floor loads. The monotonic lateral load was applied at the top level of the B2 beam.

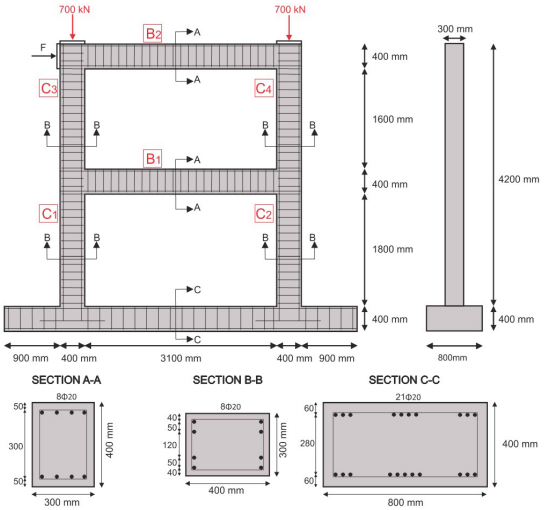

Figure 1. Geometry of the frame [27].

3 NUMERICAL SIMULATION – NLFEA

3.1 Material constitutive model

3.1.1 Concrete

The ATENA software [3] allows nonlinear finite element analysis (NLFEA) of reinforced concrete structures using the finite element method. Cracking can be represented numerically in finite elements through the crack band approach [15]. This approach assumes that the fracture processes occur along a band that coincides with the position of the crack.

Concrete behavior is simulated through the fracture-plastic constitutive model [28], which considers the phenomena of cracking and plasticity and adopts strains decomposition by adding the elastic (ε_{ij}^{e}), plastic (ε_{ij}^{p}), and fracture (ε_{ij}^{f}) given by Equation 1:

$$\varepsilon_{ij} = \varepsilon_{ij}^{e} + \varepsilon_{ij}^{p} + \varepsilon_{ij}^{f} \tag{1}$$

This approach enables strains separation according to their magnitude while establishing specific behavioral patterns. The material can be either in a softening or hardening regime, depending on the level and state of applied stresses. When concrete exceeds the elastic limit due to compressive stresses, for example, the stress-strain relationship suffers hardening, according to the model shown in Figure 2a, where $f_t{}'$ is the tensile strength, and E is the young modulus. In the pre-peak behavior, the ATENA software assumes the hardening curve proposed by Červenka et al. [3] as follows in Equation 2:

$$\sigma = f_{c0} + (f_c' - f_{c0})\sqrt{1 - \left(\frac{\varepsilon_{cp} - \varepsilon}{\varepsilon}\right)^2} \tag{2}$$

where f_c' is the compressive strength, f_{c0} is the compressive stress when the plasticity phenomenon begins, and ε_{cp} is the plastic strain.

The crack band approach allows compressive and tensile strains in the post-peak regime to be transformed into nonlinear fracture mechanics model parameters. For example, the equivalent plastic strains (ε_{eq}^{p}) and fracture strains (ε_{ij}^{f}) are transformed into plastic displacements (W_d) and crack openings (w) through the crack band size parameters L_c and L_t, respectively. The crack band size depends on the size of the finite element and the orientation of the crack within it. In general, the crack band size for L_c is calculated from the size of the element projected into the direction parallel to the crack and for L_t into the direction perpendicular to the crack. The concrete behavior after reaching compressive strength is described by the downline shown in Figure 2b, whose area under the line represents the energy dissipated during compression failure. Additionally, a scheme of how the compression band size is determined is also shown. The plastic displacement that governs the brittleness of the concrete after the peak is reached can be determined by the product of ε_{eq}^{p} and L_c. According to experimental studies developed by Van Mier [29], this parameter may be assigned as 0.5 mm for concretes with normal strength.

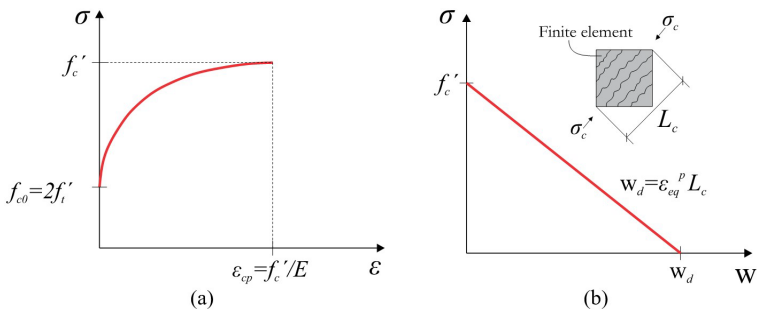

Figure 2. Compression models: a) hardening and b) softening.

Concrete compressive failure is conditioned by the triaxial failure criterion proposed by Menetrey and Willam [30]. It is represented geometrically by an envelope that defines the concrete compressive strength limit under the confinement effect. Figure 3a shows the axes σ_1, σ_2, and σ_3 corresponding to the principal compressive stresses. The failure surface around the hydrostatic axis (σ1=σ2=σ3) is also presented. The parameters σ_0 and τ_0 associated with vectors contained in the hydrostatic axis and the deviatoric plane correspond to the hydrostatic compression stress and the deviatoric shear stress, respectively. Failure occurs when, for a given confinement level σ_0, the deviatoric shear stress τ_0 reaches the failure surface [31].

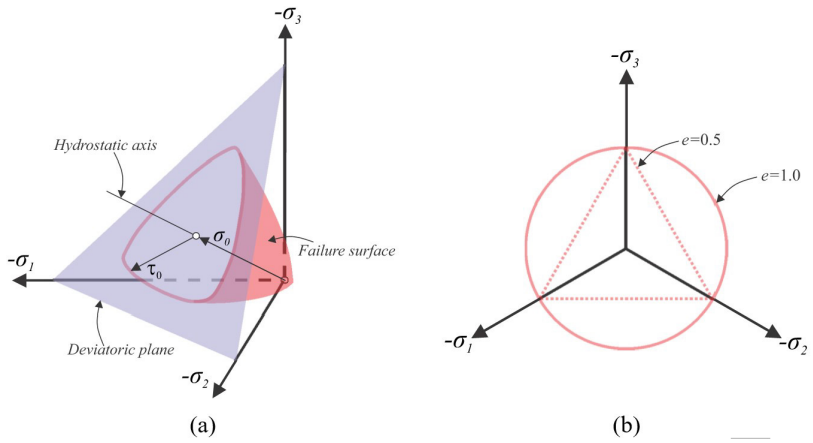

Figure 3. (a) Menétrey-Willam failure surface and (b) eccentricity [30].

The failure criterion proposed by Menetrey and William [30] incorporated into the ATENA material model is governed by Equation 3:

$$F(\xi,\rho,\theta)=\left[\sqrt{1.5}\frac{\rho}{f_c'}\right]^2+m\left[\frac{\rho}{\sqrt{6}f_c'}r(\theta,e)+\frac{\xi}{\sqrt{3}f_c'}\right]-c=0 \tag{3}$$

where ξ and ρ are the hydrostatic and deviatoric stress invariants, respectively; θ is the deviatoric polar angle, and f_c' the axial compressive strength. Additionally, c and m are the friction and cohesion parameters of the material. The dimensionless parameter e in the elliptic function $r(\theta,e)$ proposed by Klisinski [32] is known as eccentricity, and it allows the adjustment of the geometry of the surface (Figure 3b), being able to vary from a triangular (e=0.5) to a circular shape (e=1).

Tensile behavior is described by the Hordijk softening function [33]. Figure 4 shows the dissipated energy once the material reaches maximum tensile strength, whereby the area under the curve is known as the fracture energy (G_F). The curve is described by Equation 4:

$$\frac{\sigma}{f_t}=\left\{1+\left(c_1\frac{w}{w_c}\right)^3\right\}\exp\left(-c_2\frac{w}{w_c}\right)-\frac{w}{w_c}(1+{c_1}^3)\exp\left(-c_2\right) \tag{4}$$

where σ is the normal tensile stress at the crack band, f_t is the tensile strength, w is the crack opening, and w_c is the crack opening once energy has been completely dissipated.

The c_1 and c_2 parameters are experimentally validated adjustment coefficients whose values are equal to 3 and 6.93, respectively. The value of w_c can be estimated by Equation 5:

$$w_c=5.14\frac{G_F}{f_t} \tag{5}$$

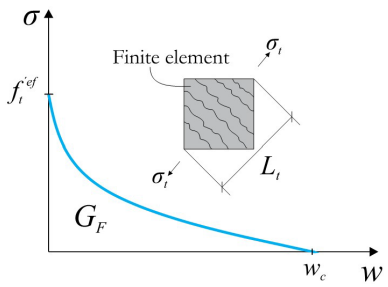

Figure 4. Tensile softening model according to Hordijk [33].

The shear stiffness (K_s) developed along the crack faces due to aggregate interlocking is considered by ATENA. It is calculated using Equation 6, where the normal stiffness of the crack plane (K_w) is multiplied by a parameter known as the shear factor (S_F). The shear factor relates the simultaneous action of the fracture on mode I (opening) and mode II (sliding). Based on a fit of experimental data, the ATENA software [3] recommends a value of 20 for conventional concrete. However, the shear stiffness can be influenced by aspects such as the type of aggregate, aggregate size, and the roughness of the crack faces. Therefore, values different from the recommended one may be used depending on the properties of the simulated concrete.

$$K_s = S_F K_w \tag{6}$$

3.1.2 Reinforcement

The constitutive model of concrete reinforcement followed a multilinear stress-strain relationship, whereby the behavior of steel bars is defined according to points of the tensile curve, where f_1 is the yield strength, f_2 and f_3 are the hardening strength, and f_4 is the ultimate stress of the steel, as shown in Figure 5. The function is also valid for bars subjected to compressive stress. Depending on these points, the model may also consider steel yielding and plastic hardening. For determining the behavior of steel bars, at least three parameters must be set, namely: elastic modulus (E_s), yield stress (f_y) and the failure point coordinates.

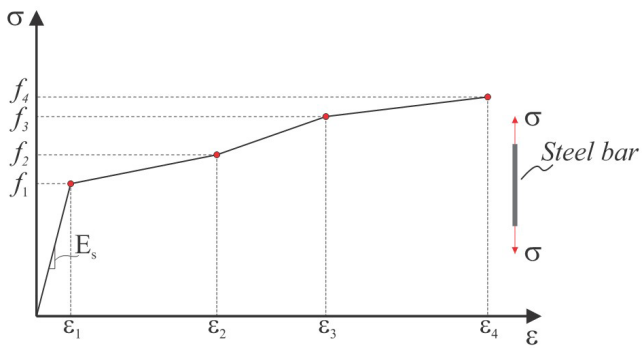

Figure 5. Multilinear stress-strain relationship.

The reinforcement was modeled with a discrete approach using truss elements incorporated into the concrete mesh. This element type only admits tensile and axial compression stresses, disregarding flexural and shear stiffness. However, the reinforcement slip caused by the debonding is considered by means of the fictitious interface composed of bond-link elements that connect the nodes of the truss and the concrete. When the maximum bond strength is reached, a relative slip is generated between the truss nodes and the concrete, and automatically a new nodal displacement is calculated for the reinforcement. In ATENA, it is possible to define a bond-slip function based on the CEB-FIP Model Code [34].

3.2 Problem setup

The numerical simulation of the reinforced concrete frame consisted of a bidimensional (2D) model. The model showed a closer capacity load with the real behavior when adopting a shear factor (S_f) of 50, and a value of fracture energy (G_f) close value to that expressed in the CEB-FIP Model Code [35]. Plastic strain at the compressive strength (ε_c^p) and bond-slip curve (good bond with $\tau_{max} = 10$ MPa) were determined according to the CEB-FIP Model Code 90 [34]. Default values were used, such as reduction factor for compressive strength and strength at the onset of nonlinear behavior (f_{co}) in the ATENA software [3]. Table 1 presents the variables used in the numerical simulation-NLFEA.

Table 1. Mechanical properties of concrete and steel

Parameter	Concrete	Long. Steel	Transv. Steel	Reference
Elastic Modulus - E	23674 MPa	192500 MPa	200000 MPa	[27]
Hardening modulus - E_{sh}	/	3100 MPa	3100 MPa	[27]
Fracture energy - G_f	90 N/m	/	/	[35]
Shear factor - S_f	50	/	/	adopted
Compression strength - f_c	30 MPa	/	/	[27]
Tensile strength - f_t	1.81 MPa	/	/	[27]
Strength at onset of nonlinear behavior - f_{co}	3.6 MPa	/	/	[3]
Plastic strain at compressive strength - ε_c^p	0.00185	/	/	[34]
Reduction factor of the compressive strength	0.8	/	/	[3]
Yield strength - f_y	/	418 MPa	596 MPa	[27]
Ultimate strength - f_u	/	454 MPa	640 MPa	[27]
Yield strain - ε_s	/	0.00217	0.00298	[27]
Strain hardening - ε_{sh}	/	0.0095	0.0095	[27]
Ultimate strain - ε_u	/	0.0669	0.0695	[27]

Two load stages were used to perform numerical simulations under the same experimental conditions. In the first stage, a 700 kN vertical load was applied to 40 mm steel plates located in the upper face of C3 and C4 through force-controlled static analysis. In the second stage, a 140 mm horizontal displacement with 0.8 mm increments was applied to fixed steel plates connected to the C3 sideline through displacement-controlled quasi-static analysis, while the vertical forces of 700 kN applied in the first stage remained constant (Figure 6). The base of the structure was vertically and horizontally fixed. Iterative procedures were performed according to the modified Newton-Raphson method. The convergence criteria were as follows: 1% for displacement error, residual force, and absolute residual force, and 0.1% for energy error.

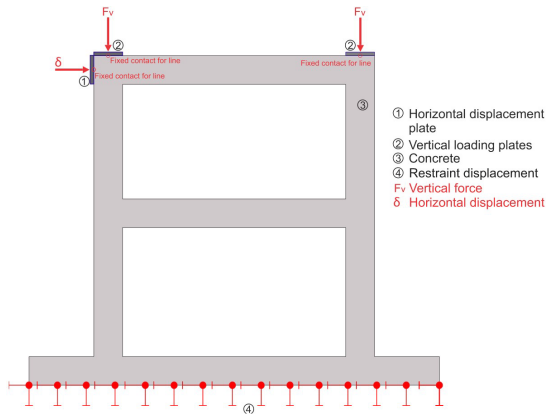

Figure 6. Boundary conditions scheme used in the numerical simulation.

Concrete was simulated with the 2D-NonlinearCementitious2 material model, using the four-node quadrilateral linear finite element with four integration points. In turn, longitudinal and transversal steel were simulated with the CCReinforcement material model using the two-node truss finite element with one integration point. Steel plates for vertical load and lateral displacement were simulated with CC3DElastIsotropic using the four-node quadrilateral linear finite element with four integration points.

Three simulations with coarse, medium and fine mesh were performed to evaluate the finite element mesh sensibility, investigating the option that best approximates the experimental results. The coarse mesh model used 100×100 mm elements, corresponding to 824 quadrilateral elements, 994 linear elements, and 2186 nodes. The medium mesh employed an 80×80 mm element size, resulting in 1262 quadrilateral elements, 994 linear elements, and 2670 nodes. Finally, the fine mesh model employed 50×50 mm elements, which correspond to 3272 quadrilateral elements, 994 linear elements, and 4845 nodes, as shown in Figure 7.

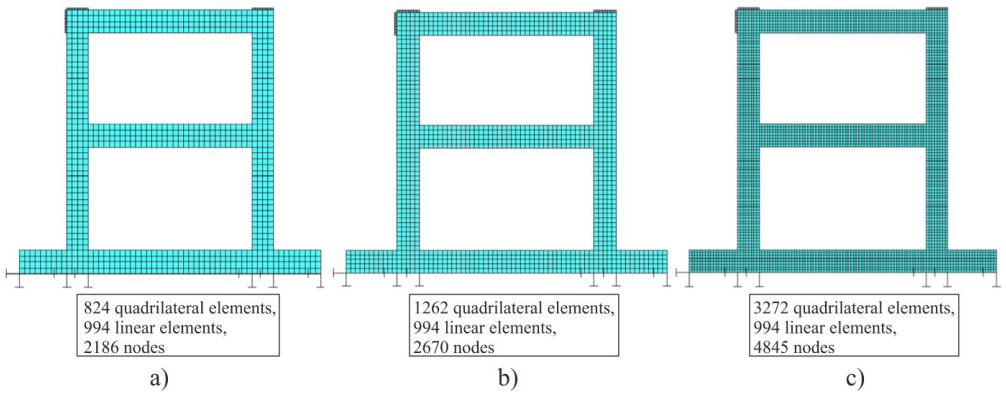

Figure 7. Discretization of finite element model with a) coarse mesh (824 quadrilateral elements, 994 linear elements, and 2186 nodes), b) medium mesh (1262 quadrilateral elements, 994 linear elements, and 2670 nodes), and c) fine mesh (3272 quadrilateral elements, 994 linear elements, and 4845 nodes).

4 NUMERICAL SIMULATION – NLSA

The nonlinear static analysis is based on consecutive static analyses ($F = KU$) in which the forces and displacements are accumulated and the stiffnesses of the beam's and column's segments are updated. This work considers only the stiffness loss due to bending moment, disregarding cracks due to shear stress.

The nonlinear static analysis is conformed by two main contributions: optimized frame finite element stiffness matrix and the axial-force-moment-curvature relationship. Unlike the frame finite element stiffness matrix, the optimized frame finite element stiffness matrix allows splitting beams and columns into segments without increasing the number of degrees of freedom of the system. The segmentation of beams and columns makes it possible to represent the stiffness loss of the structure more adequately and, consequently, its nonlinear behavior. This work uses a new expression for determining the stiffness matrix of a frame finite element of variable stiffness named optimized frame finite element stiffness matrix, shown in Equations 7-13. This way, the different levels of cracking (different stiffnesses) in an element are considered without adding degrees of freedom along the same elements. Further details and mathematical formulations of the method can be found in Martínez [36].

$$K = \begin{bmatrix} \frac{1}{C_1} & 0 & 0 & \frac{-1}{C_1} & 0 & 0 \\ 0 & \frac{C_3}{C} & \frac{C_2}{C} & 0 & \frac{-C_3}{C} & \frac{C_6}{C} \\ 0 & \frac{C_2}{C} & \frac{C_2 L - C_5}{C} & 0 & \frac{-C_2}{C} & \frac{C_5}{C} \\ \frac{-1}{C_1} & 0 & 0 & \frac{1}{C_1} & 0 & 0 \\ 0 & \frac{-C_3}{C} & \frac{-C_2}{C} & 0 & \frac{C_3}{C} & \frac{-C_6}{C} \\ 0 & \frac{C_6}{C} & \frac{C_5}{C} & 0 & \frac{-C_6}{C} & \frac{C_6 L - C_5}{C} \end{bmatrix} \quad (7)$$

$$C_1 = l\sum_{i=1}^{n}\frac{1}{E_i A_i} \tag{8}$$

$$C_2 = \frac{l^2}{2}\sum_{i=1}^{n}\frac{1}{E_i I_i} + l^2\sum_{i=1}^{n-1}\frac{1}{E_{i+1} I_{i+1}} \tag{9}$$

$$C_3 = l\sum_{i=1}^{n}\frac{1}{E_i I_i} \tag{10}$$

$$C_5 = \frac{l^3}{6}\sum_{i=1}^{n}\frac{1}{E_i I_i} + \frac{l^3}{2}\sum_{i=1}^{n}\frac{n-1}{E_i I_i} + l^3\sum_{i=1}^{n-2}\frac{(n-1)i-i^2}{E_{i+1} I_{i+1}} \tag{11}$$

$$C_6 = \frac{l^2}{2}\sum_{i=1}^{n}\frac{1}{E_i I_i} + l^2\sum_{i=1}^{n-1}\frac{1}{E_i I_i} \tag{12}$$

$$C = C_2 C_6 - C_3 C_5 \tag{13}$$

where K is the optimized frame finite element stiffness matrix, l is the segment's length, n is the number of segments of each beam or column, E_i is the elastic modulus of segment i, I_i is the moment of inertia of segment i, and A_i is the cross-sectional area of segment i.

On the other hand, the slope of the axial-force-moment-curvature diagram corresponds to the tangent stiffness (EI) of the section. It is used to update the stiffness of each segment in each new load application according to the accumulated axial force and bending moment. In the same way, the axial force-moment-curvature relationship of each section of the structure is updated in each new load application according to the accumulated axial force in each element. Several works related to the calculus of the moment-curvature relationship of a reinforced concrete section have been published [37]–[44].

In this work was used the model of Bazant and Oh [40], which suggests concrete with nonzero tension capacity and is represented by a stress-strain relationship that considers the progressive micro-cracking due to strain softening (Figure 8). In the model, a succession of ε_{cm} values increasing in small increments is considered to calculate the moment-curvature diagram of an axial force. For each of them, depth kd to the neutral axis is obtained from Equation 14. Then, the bending moment and curvature are calculated as follows in Equations 15 and 16, respectively:

$$N = k_1 f_c' bkd + \sum_{j=1}^{2}\sigma_{sj} A_{sj} - k_3 f_t' b(h - kd) \tag{14}$$

$$M = k_1 f_c' bkd\left(\frac{h}{2} - k_2 kd\right) + \sum_{i=1}^{2}\sigma_{si} A_{si}\left(\frac{h}{2} - d_i\right) + k_3 f_t' b(h - kd)\left[\frac{h}{2} - k_4(h - kd)\right] \tag{15}$$

$$k = \frac{\varepsilon_{cm}}{kd} \tag{16}$$

where k_1, k_2 are compressive stress parameters (see ref [40]); k_3, k_4 are tensile stress parameters (see ref [40]); f_c' is the compression strength of concrete; f_t' is the direct tensile strength of concrete; ε_{cm} is the strain of concrete at the compression face; b is the cross-section width; kd is the depth to the neutral axis; d is the depth to tensile reinforcement; $\sigma_{sj}; \sigma_{si}$ are the stresses of compression and tension reinforcement; and A_{s1}, A_{s2} are the areas of compression and tension reinforcement.

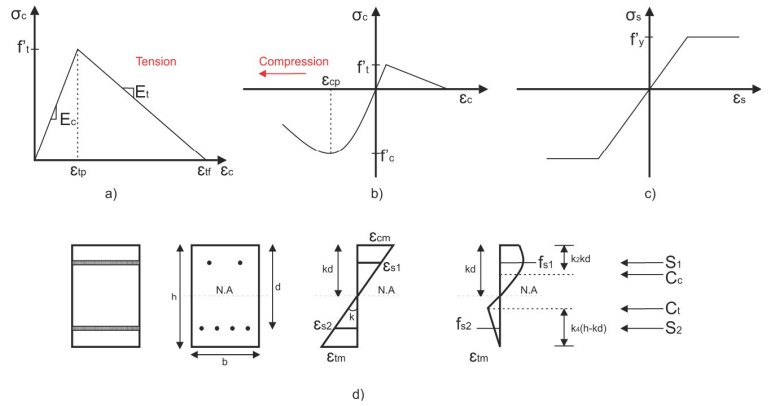

Figure 8. Uniaxial stress-strain relations for concrete in (a) tension and (b) compression, (c) for steel, and (d) stress-strain distributions in the beam cross-section [40].

As discussed above, the slope of the axial-force-moment-curvature diagram corresponds to the tangent stiffness (EI) of the section. Therefore, the algorithm developed in this work considers the axial-force-moment-curvature relationship previously calculated at each new load application and creates a bending moment vs percentage of the initial stiffness table, as shown in the schematic of Figure 9. The algorithm uses the table to assign the corresponding EI value to each segment to generate the stiffness matrix of each element and consecutively the structure's stiffness matrix, following the equation $F = KU$. F refers to external forces applied to the structure, K is the global stiffness matrix of the structure, and U are the degrees of freedom of the structure. In this way, the mechanical and geometric properties of the reinforced concrete sections (concrete and steel) are considered when is updated the tangent stiffness EI of each segment in the coefficients $C_1 - C_6$ (Equations 8-12) of the element's stiffness matrix.

This process is repeated until the accumulated moment in any segment of the structure exceeds the maximum moment of its axial force-moment-curvature relationship, as shown in Figure 10.

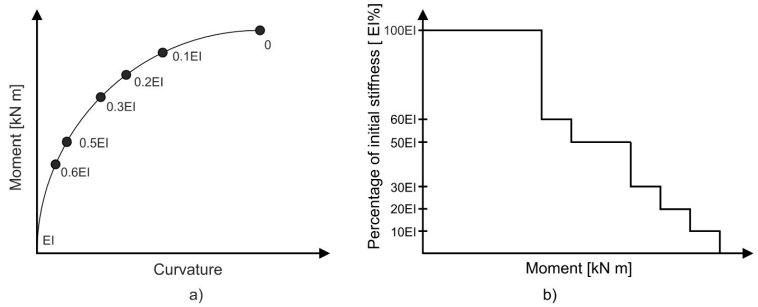

Figure 9. Scheme of a) moment-curvature, b) initial stiffness variation-moment.

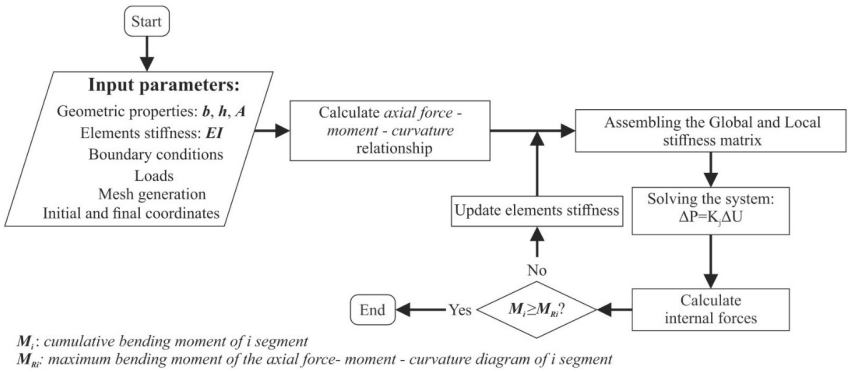

Figure 10. Scheme of the numerical simulation using NLSA.

In the numerical simulation NLSA, when the structure was discretized with more than 60 segments, there were no significant differences in the results; therefore, the beams and columns were discretized in 14 and 16 segments, respectively (Figure 11). The methodology used 0.8 kN increments.

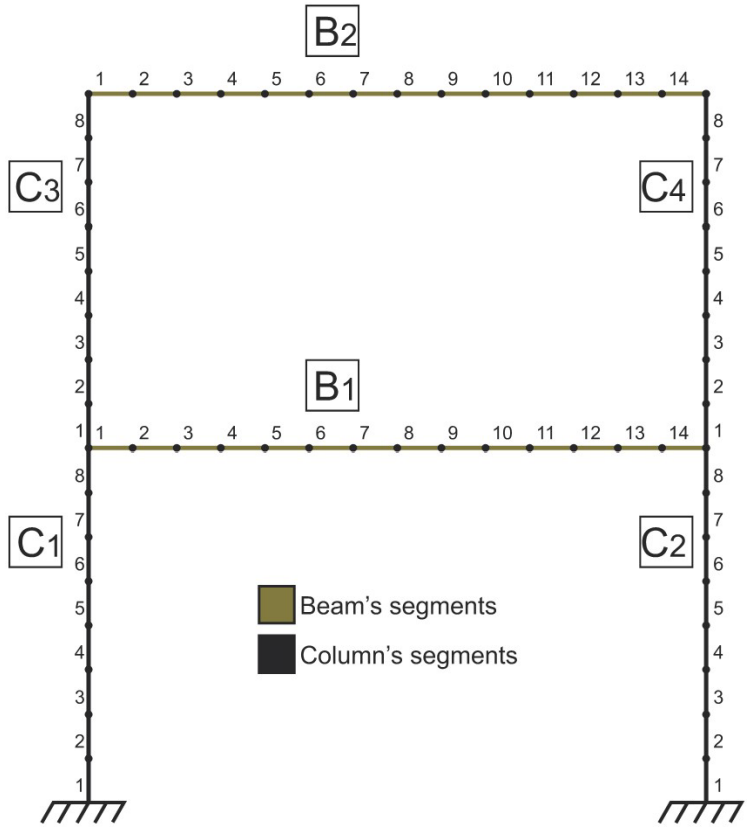

Figure 11. Discretization of beams and columns (60 segments).

5 VALIDATION OF RESULTS AND DISCUSSIONS

5.1 Numerical simulation NLFEA, numerical simulation NLSA, and experimental test

Table 2 presents the capacity load values of experimental and numerical simulation NLFEA with fine, medium, and coarse mesh for a horizontal displacement of 7.8 cm. In contrast, Figure 12 presents the cracking panoramas of each model NLFEA. Although the three simulations have shown cracks in the same regions, it is possible to observe that the parameters presented and a fine mesh model in the ATENA program allowed the capacity load closest to the experimental value since the stiffness and capacity load increased as the finite element size increased.

Table 2. Ultimate load for experimental and numerical analysis.

Model	Mesh size	Ultimate load [kN]	Error [%]
Experimental test		332	---
Coarse mesh	100 mm	345.1	3.8
Medium mesh	80 mm	340.9	2.6
Fine mesh	50 mm	332.8	0.24

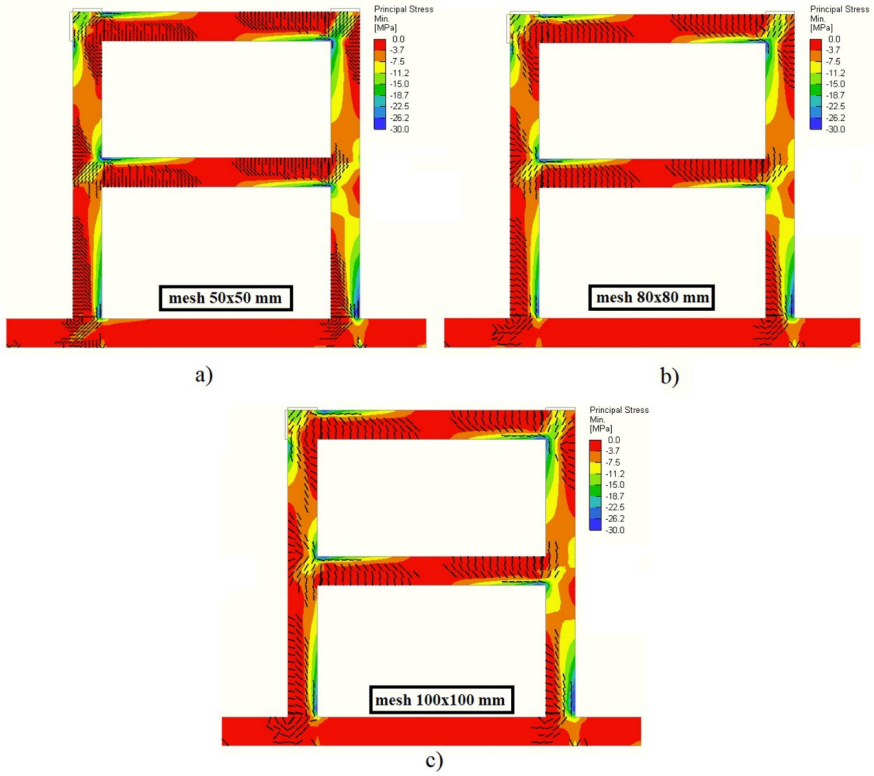

Figure 12. Crack patterns of the frame for (a) fine, (b) medium, and (c) coarse mesh, with a 7.8 cm lateral displacement.

Figures 13 and 14 show the comparison of cracking of the beam-column joint (B2-C3) and C1 column base with the experimental test, respectively. The fine mesh model presented a higher concentration of cracks due to the greater discretization of the mesh. However, all the models showed similarities with the cracking experimental. Thus, further comparisons with NLSA were performed using the fine mesh model.

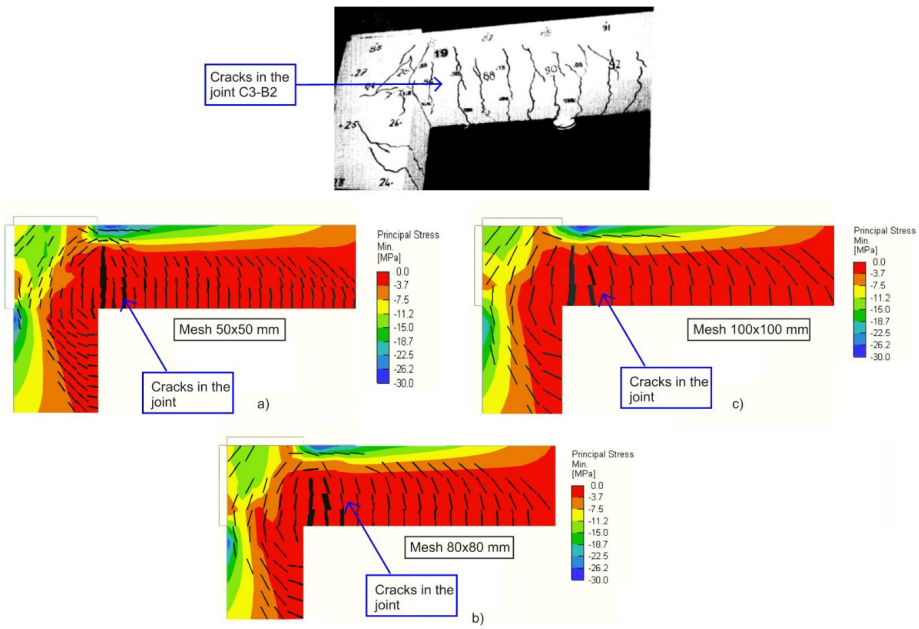

Figure 13. Crack patterns of the beam-column joint (B2-C3) for (a) fine, (b) medium, and (c) coarse mesh, with a 7.8 cm lateral displacement.

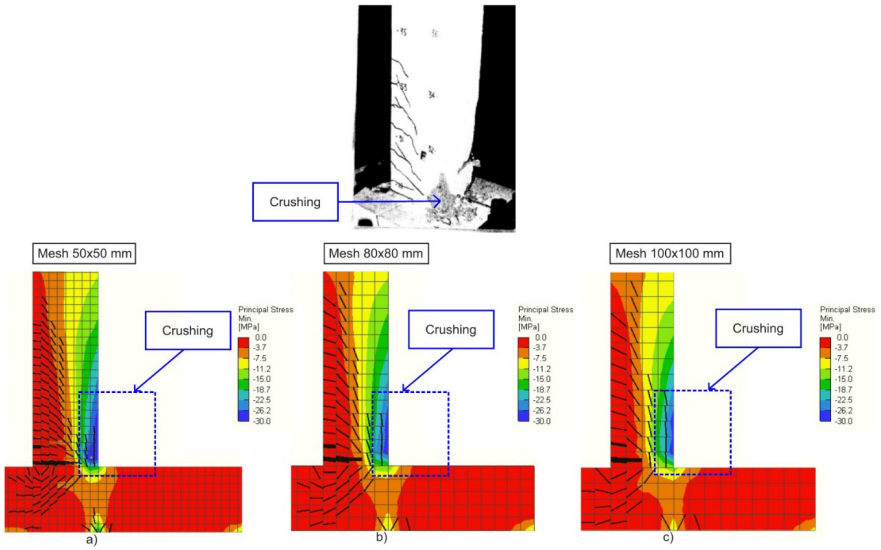

Figure 14. Crushing in the base of C1 column for (a) fine, (b) medium, and (c) coarse mesh, with a 7.8 cm lateral displacement.

The ultimate load in the experimental analysis occurred at 332 kN. The load was equal to 332.8 kN and 344 kN in the numerical simulation using NLFEA and NLSA, respectively, corresponding to differences of 0.24% and 3.6% (Table 2). As shown in Figure 15, the numerical simulation with NLFEA and NLSA presented closer results when compared with the experimental test; however, the NLFEA showed a better agreement. Future analysis in the numerical simulation NLSA considering the role of geometrical nonlinearity could be developed to analyze its contribution to the calibration of the capacity curve. The results obtained in this study were compared with those of other authors [14], [17].

The numerical simulation using NLFEA and NLSA presented continuous stiffness loss and cracking in the elements, as evidenced in the experimental test. The NLSA finished with 430 load steps, reaching the maximum moment in the C2 base. Figure 16 illustrates all elements with 100% stiffness (without load applied). Table 3 shows the results obtained in the concrete beams and columns, while Table 4 presents the values achieved in the longitudinal bars.

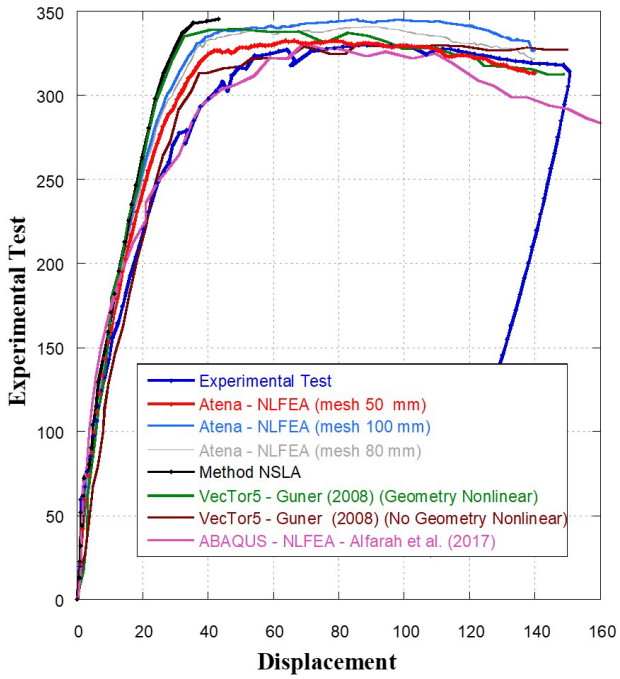

Figure 15. Capacity curve comparison (experimental, numerical simulation NLFEA (Atena) and NLSA, and other authors) [14], [17].

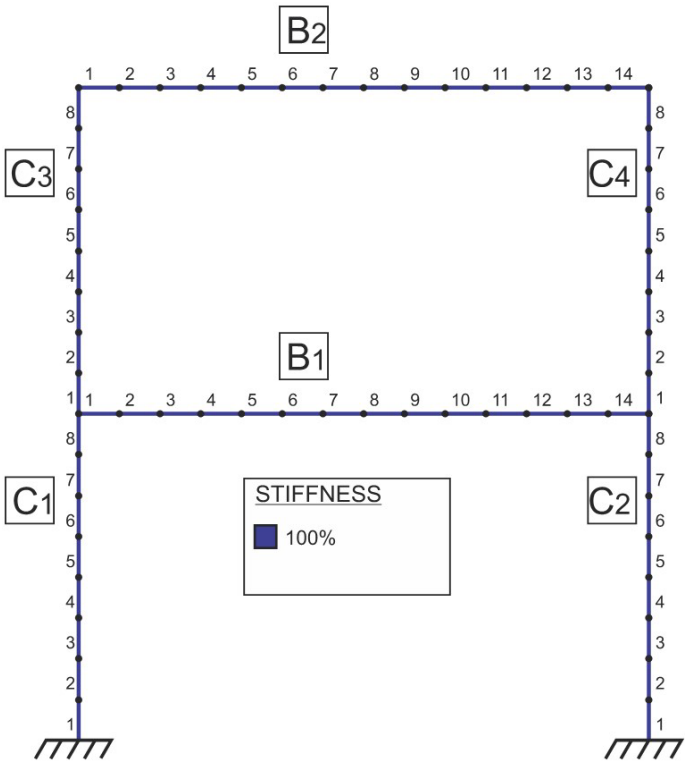

Figure 16. Discretization of the frame with 100% stiffness (without stiffness loss) [36].

Table 3. Comparison of results obtained in the concrete beams and columns.

Element	Numerical result -NLFEA	Numerical result -NLSA	Experimental result
Flexural cracks in the beam B1	59.4 kN (Figure 17a)	61.6 kN – elements 1 and 14, stiffness: 41% (Figure 17b)	52.5 kN
Flexural cracks at the base of the columns	152.8 kN (Figure 18a)	145 kN – element 1, column C1, stiffness: 43% 145 kN – element 1, column C2, stiffness: 50% (Figure 18b)	145 kN

Table 4. Comparison of results obtained in the longitudinal bars.

Element	Numerical result - NLFEA	Numerical result -NLSA	Experimental result
Yielding in the longitudinal reinforcement of beam B1	281.5 kN (Figure 19a)	302.4 kN – element 1, stiffness: 0.75%	264 kN (top)
		302.4 kN – element 14, stiffness: 0.85% (Figure 19b)	287 kN (bottom)
Yielding in the longitudinal reinforcement of column	326.1 kN (Figure 20a)	320 kN – element 1, column C1, stiffness: 0.81%	323 kN
		335.2 kN – element 1, column C2, stiffness: 2.7% (Figure 20b)	
Yielding in the longitudinal reinforcement of beam B2	326.1 kN (Figure 20a)	340.8 kN – element 1, stiffness: 1.0%	329 kN
		340.8 kN – element 14, stiffness: 0.75% (Figure 21)	

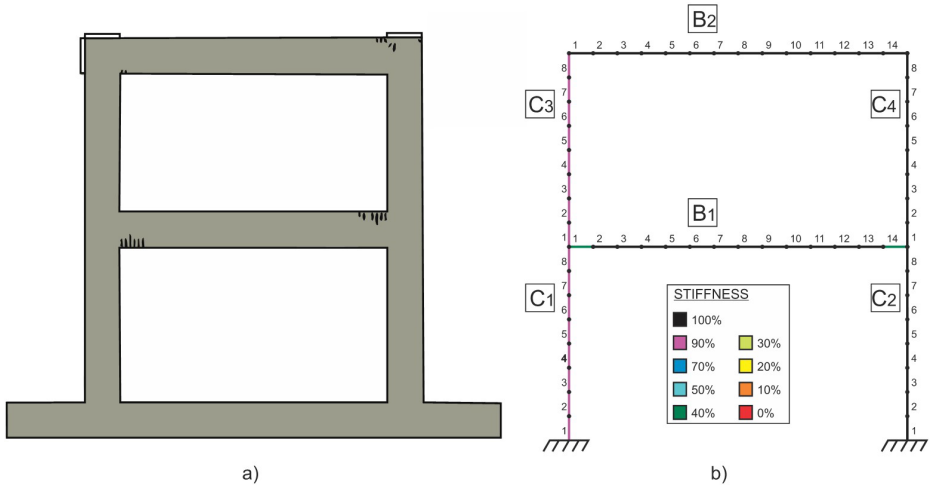

Figure 17. Flexural cracks at the B1 beam according to the (a) numerical simulation at a 59.4 kN load and (b) the percentage of stiffness at a 61.6 kN load.

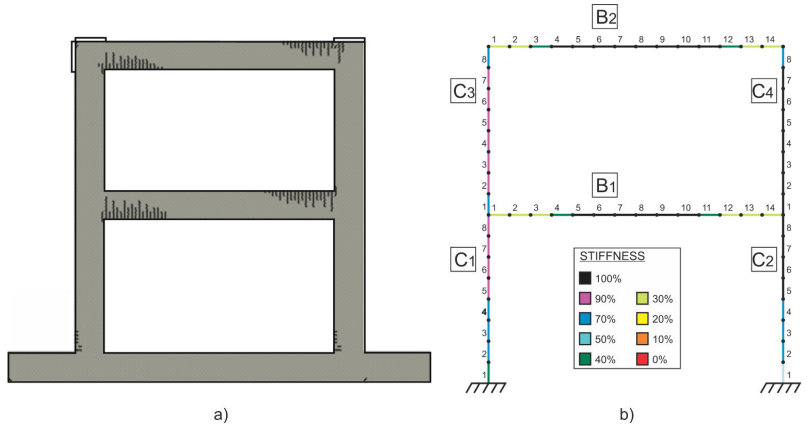

Figure 18. Flexural cracks at the base of columns according to (a) numerical simulation at a 152.8 kN load and (b) the percentage of stiffness at a 145 kN load.

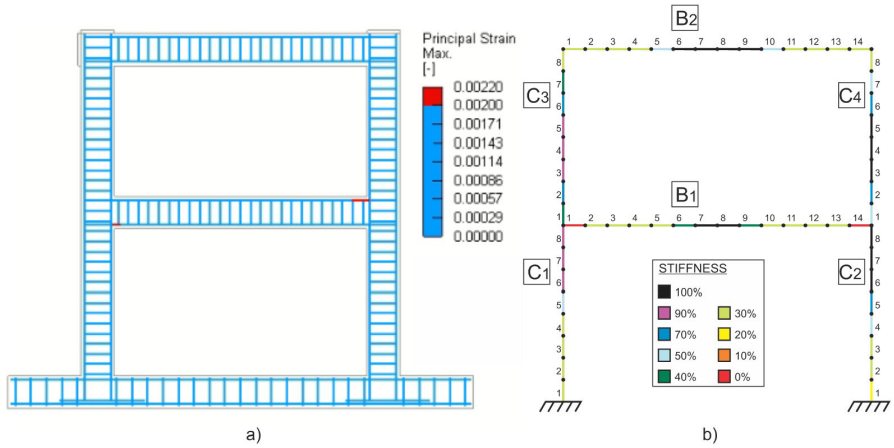

Figure 19. Longitudinal steel yielding at the B1 beam ends: (a) numerical simulation at a 281.5 kN load and (b) the percentage of stiffness at a 302.4 kN load.

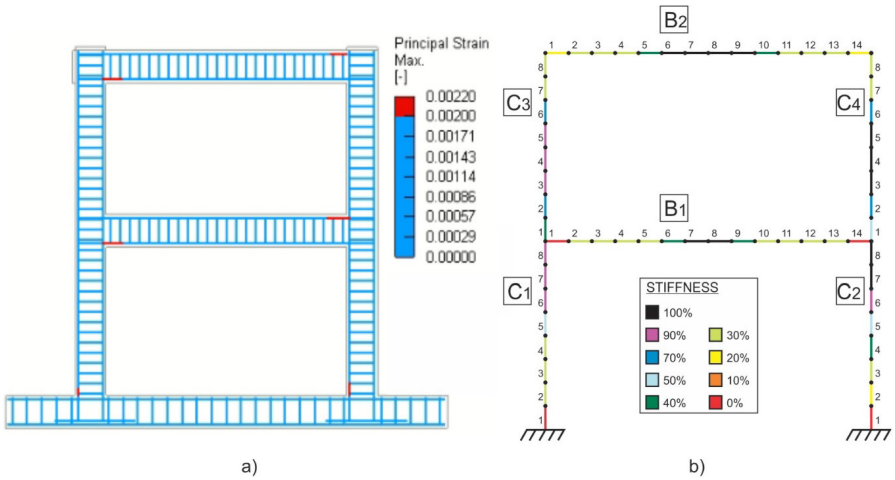

Figure 20. Longitudinal steel yielding at columns base: (a) numerical simulation at a 326.1 kN load and (b) the percentage of stiffness at a 335.2 kN load.

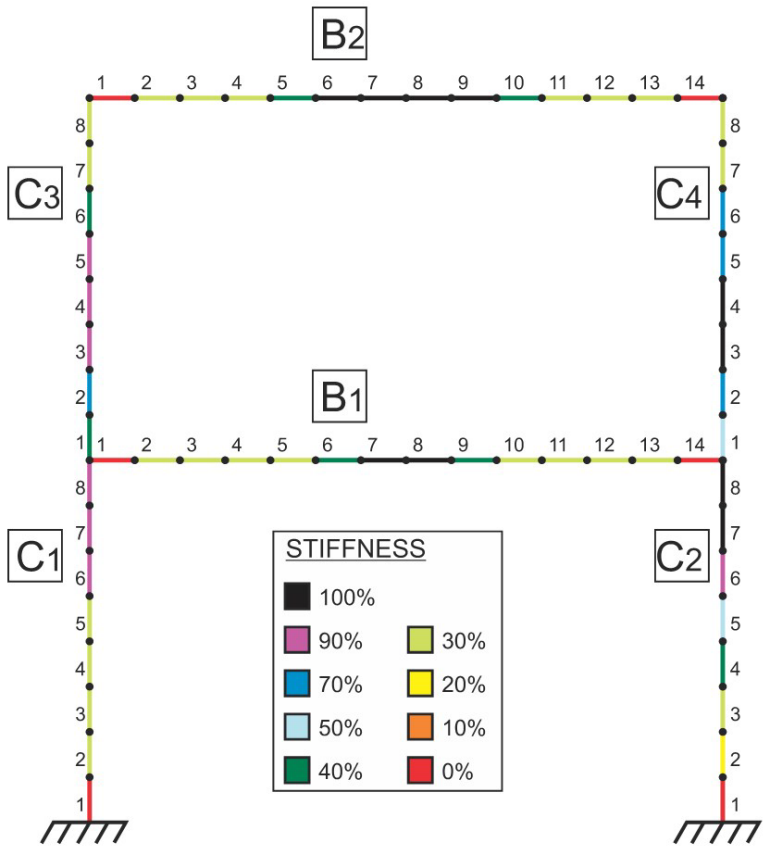

Figure 21. Percentage of stiffness at a 340.8 kN load.

The NLSA allows the determination of the stiffness loss history in all structure elements for each load step (Figure 22). The results showed that B1 beam was the most critical for stiffness loss, followed by B2 beam and C1 and C2 columns, while C3 and C4 columns presented less structural damage. These results are consistent with the behavior obtained in the numerical simulation NLFEA and experimental test, demonstrating the expression to determine the stiffness matrix proposed is adequate to represent the stiffness loss and ultimate capacity load of reinforced concrete elements.

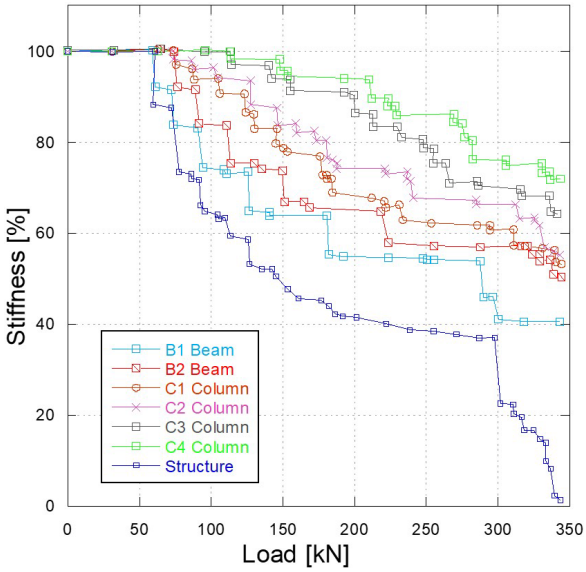

Figure 22. Stiffness loss sequence.

6 CONCLUSIONS

In this study, nonlinear methodologies for studying the structural behavior of a reinforced concrete frame subjected to monotonic load were analyzed through a numerical simulation with nonlinear finite element analysis (NLFEA) and a numerical simulation with optimized nonlinear static analysis (NLSA). Equations for determining the optimized frame finite element stiffness matrix in the NLSA were presented. Based on the results of the validation, this study allows us to infer that:

- The ultimate loads obtained in the fine-mesh numerical simulation NLFEA and NLSA were close to those obtained in the experimental test. The numerical simulation NLFEA showed good accuracy regarding crack patterns and longitudinal steel yielding due to adequate parameters and mesh discretization. These findings indicate that both analyses could be employed to study reinforced concrete elements cracking.
- The numerical simulation NLSA with stiffness degradation allowed the analysis of the nonlinear behavior of reinforced concrete elements with monotonic lateral and constant vertical loads. The stiffness loss observed in the numerical simulation NLSA showed the same sequence as those verified in the experimental test and numerical simulations by finite elements.
- The model proposed by Bazant and Oh [40] for determining the moment–curvature diagram in the numerical simulation NLSA showed a higher ultimate load for the capacity curve than the experimental test.
- When applied to the reinforced concrete, the numerical simulation NLSA indicated the low-stiffness regions (cracked zones) and ultimate load in the structure – important parameters for the structural design. The most critical section in the frame was the B1 beam, showing the first cracks and stiffness loss.
- The numerical simulation with NLFEA can reproduce the nonlinearity behavior of structural elements using material nonlinearity, bonding properties, and boundary conditions. However, it is worth highlighting that it requires a high computational cost.
- The numerical simulation NLSA allows discretizing beams and columns in segments without increasing degrees of freedom along the element through the utilization of an optimized frame finite element stiffness matrix, simplifying the calculation of the results in the structure.
- Future research, including geometrical nonlinearity in the numerical simulation with NLSA is recommended to be developed to compare its influence on the results.

ACKNOWLEDGEMENTS

The authors greatly appreciate the financial support provided by the Brazilian National Council for Scientific and Technological Development (CNPq) (Grant 141517/2021-2).

REFERENCES

[1] Dassault Systèmes, *Simulia. Dassault Systèmes Documentation SIMULIA 2017*. Rhode Island: Abaqus, 2017.

[2] ANSYS, Inc., *ANSYS Documentation*. Canonsburg, PA, USA: ANSYS, Inc., 2019.

[3] V. Červenka, L. Jendele, and J. Červenka, *ATENA Program Documentation Part 1: Theory*. Prague: Červenka Consulting, 2021.

[4] DIANA FEA, *DIANA User's Manual – Release 10.6*. Delft: DIANA FEA, 2021.

[5] T. Belytschko and T. Black, "Elastic crack growth in finite elements with minimal remeshing," *Int. J. Numer. Methods Eng.*, vol. 45, pp. 601–620, Jun. 1999, http://dx.doi.org/10.1002/(SICI)1097-0207(19990620)45:5<601:AID-NME598>3.0.CO;2-S.

[6] M. M. H. Mousum and A. R. M. Islam, "Review on X-FEM for fracture mechanics: current developments and future prospects," in *Inter. Conf. Mech. Eng. Renewable Ener – ICMERE*, 2015, pp. 1–6.

[7] A. Yazid, N. Abdelkader, and H. Abdelmadjid, "A state-of-the-art review of the X-FEM for computational fracture mechanics," *Appl. Math. Model.*, vol. 33, no. 12, pp. 4269–4282, Dec. 2009, http://dx.doi.org/10.1016/j.apm.2009.02.010.

[8] R. E. Goodman, R. L. Taylor, and T. L. Brekke, "A model for the mechanics of jointed rock," *J. Soil Mech. Found. Div.*, vol. 94, no. 3, pp. 637–659, May 1968, http://dx.doi.org/10.1061/JSFEAQ.0001133.

[9] A. Martínez, J. Liaudat, C. M. López, and I. Carol, "3D zero-thickness interface model for fracture of cement-based materials with chemical degradation," *Int. J. Solids Struct.*, vol. 238, pp. 111379, Mar. 2022, http://dx.doi.org/10.1016/j.ijsolstr.2021.111379.

[10] V. D. Garolera, P. I. Aliguer, J. M. Segura, I. Carol, M. R. Lakshmikantha, and J. Alvarellos, "Zero-thickness interface elements with HM coupling, formulation and applications in geomechanics," in *Proc. XII Int. Conf. Comput. Plasticity: Fundam. Appl. – CIMNE*, 2013, pp. 1372–1383.

[11] G. D. Dhadse, G. D. Ramtekkar, and G. Bhatt, "Thin layer interface: an alternative to zero thickness interface for modeling of footing-soil interaction system," *J. Build. Pathol. Rehabil.*, vol. 7, no. 1, pp. 50, May 2022, http://dx.doi.org/10.1007/s41024-022-00190-1.

[12] O. L. Manzoli, A. L. Gamino, E. A. Rodrigues, and G. K. S. Claro, "Modeling of interfaces in two-dimensional problems using solid finite elements with high aspect ratio," *Comput. Struc.*, vol. 94, pp. 70–82, Mar. 2012, http://dx.doi.org/10.1016/j.compstruc.2011.12.001.

[13] O. L. Manzoli et al. Modeling of multiple cracks in reinforced concrete members using solid finite elements with high aspect ratio, in Computational Modelling of Concrete Structures, Boca Raton: CRC Press, 2014, Vol. 1, pp. 383–392. http://hdl.handle.net/11449/117341 (accessed June 30, 2023).

[14] B. Alfarah, F. López-Almansa, and S. Oller, "New methodology for calculating damage variables evolution in plastic damage model for RC structures," *Eng. Struct.*, vol. 132, pp. 70–86, Feb. 2017, http://dx.doi.org/10.1016/j.engstruct.2016.11.022.

[15] J. Lubliner, J. Oliver, S. Oller, and E. Oñate, "Plastic-damage model for concrete," *Int. J. Solids Struct.*, vol. 25, no. 3, pp. 299–326, Sep. 1989, http://dx.doi.org/10.1016/0148-9062(89)91126-1.

[16] J. Lee and G. L. Fenves, "Plastic-damage model for cyclic loading of concrete structures," *J. Eng. Mechanics*, vol. 124, no. 8, pp. 892–900, Aug. 1998, https://doi.org/10.1061/(asce)0733-9399(1998)124:8(892).

[17] S. Guner, "Performance assessment of shear-critical reinforced concrete plane frames," Ph.D. dissertation, Dept. Civil Eng., Univ. Toronto, Toronto, Canada, 2008.

[18] F. J. Vecchio and M. P. Collins, "Modified compression-field theory for reinforced concrete elements subjected to shear," *ACI J.*, vol. 83, no. 2, pp. 219–231, Jan. 1986, http://dx.doi.org/10.14359/10416.

[19] P. L. Ng, J. Y. K. Lam, and A. K. H. Kwan, "Nonlinear multilevel analysis of reinforced concrete frames," *Eng. Struct. Technol.*, vol. 7, no. 4, pp. 168–176, Apr. 2015, http://dx.doi.org/10.3846/2029882x.2016.1150793.

[20] J. Y. K. Lam, "Full-range analysis of reinforced concrete members and frames," Ph.D. dissertation, Univ. Hong Kong, Hong Kong, 2009.

[21] N. Caglar, A. Demir, H. Ozturk, and A. Akkaya, "A simple formulation for effective flexural stiffness of circular reinforced concrete columns," *Eng. Appl. Artif. Intell.*, vol. 38, pp. 79–87, Feb. 2015, http://dx.doi.org/10.1016/j.engappai.2014.10.011.

[22] C. M. Chan, N. C. Mickleborough, and F. Ning, "Analysis of cracking effects on tall reinforced concrete buildings," *J. Struct. Eng.*, vol. 126, no. 9, pp. 995–1003, Sep. 2000, http://dx.doi.org/10.1061/(asce)0733-9445(2000)126:9(995).

[23] S. Guner and F. J. Vecchio, "Pushover analysis of shear-critical frames: verification and application," *ACI Struct. J.*, vol. 107, no. 1, pp. 72–81, 2010.

[24] S. Guner and F. J. Vecchio, "Pushover analysis of shear-critical frames: formulation," *ACI Struct. J.*, vol. 107, no. 1, pp. 63–71, 2010.

[25] H. M. S. S. Hippola, K. K. Wijesundara, and R. Nascimbene, "Response of shear critical reinforced concrete frames and walls under monotonic loading," *Eng. Struct.*, vol. 251, pp. 113483, Jan. 2022, http://dx.doi.org/10.1016/j.engstruct.2021.113483.

[26] R. M. C. M. Rajapakse, K. K. Wijesundara, R. Nascimbene, C. S. Bandara, and P. B. R. Dissanayake, "Accounting axial-moment-shear interaction for force-based fibre modeling of RC frames," *Eng. Struct.*, vol. 184, pp. 15–36, Apr. 2019, http://dx.doi.org/10.1016/j.engstruct.2019.01.075.

[27] F. J. Vecchio and M. B. Emara, "Shear deformations in reinforced concrete frames," *ACI Struct. J.*, vol. 89, no. 1, pp. 46–56, Jan. 1992, http://dx.doi.org/10.14359/1283.

[28] J. Červenka and V. K. Papanikolaou, "Three-dimensional combined fracture-plastic material model for concrete," *Int. J. Plast.*, vol. 24, no. 12, pp. 2192–2220, Dec. 2008, http://dx.doi.org/10.1016/j.ijplas.2008.01.004.

[29] J. G. Van Mier, "Multiaxial strain-softening of concrete, part I: fracture," *Mater. Struct.*, vol. 19, no. 111, May 1986.

[30] P. Menetrey and K. J. Willam, "Triaxial failure criterion for concrete and its generalization," *ACI Struct. J.*, vol. 92, no. 3, pp. 311–318, May 1995, http://dx.doi.org/10.14359/1132.

[31] V. Cervenka, "Computer simulation of failure of concrete structures for practice," in *1st Int fib Congr.*, 2002, pp. 289–304.

[32] M. Klisinski, "Degradation and plastic deformation of concrete, IFTR Report 38," Ph.D. dissertation, Polish Acad. Sci., Warsaw, Poland, 1985.

[33] D. A. Hordijk, "Local approach to fatigue of concrete," Ph.D. dissertation, Dept. Civil Eng., Delft Univ. Technol., Delft, The Netherlands, 1991.

[34] Comité Euro-International du Béton, Fédération Internationale du Béton, *fib Model Code for Concrete Structures 1990*, CEB-FIB 90, 1990, https://doi.org/10.1680/ceb-fipmc1990.35430.

[35] Comité Euro-International du Béton, Fédération Internationale du Béton, *fib Model Code for Concrete Structures 2010*, CEB-FIB 2010, 2010.

[36] J. Martínez, "Análise estática não linear de estruturas de concreto armado usando a matriz de rigidez do elemento finito de pórtico otimizado," Master thesis, Dept. Civil Eng., State Univ. Campinas, Campinas, Brazil, 2020.

[37] C. P. Siess and M. A. Sozen, "Load-moment-curvature characteristics of reinforced concrete cross sections," *ACI J. Proc.*, vol. 61, no. 7, pp. 763–778, Jan. 1964.

[38] P. S. Rao and B. V. Subrahmanyam, "Trisegmental moment-curvature relations for reinforced concrete members," *ACI J. Proc.*, vol. 70, no. 5, pp. 346–351, May 1973.

[39] K. Sakai and K. Kakuta, "Moment-curvature relationship of reinforced concrete members subjected to combined bending and axial force," *ACI J. Proc.*, vol. 77, no. 3, pp. 189–194, May 1980.

[40] Z. P. Bazant and B. H. Oh, "Deformation of progressively cracking reinforced concrete beams," *J. Am. Concr. Inst.*, vol. 81, no. 3, pp. 268–278, Nov. 1984, http://dx.doi.org/10.1016/0010-4485(84)90120-9.

[41] W. A. M. Alwis, "Trilinear moment-curvature relationship for reinforced concrete beams," *ACI Struct. J.*, vol. 87, no. 3, pp. 276–283, Jan. 1990.

[42] H. G. Kwak and S. P. Kim, "Nonlinear analysis of RC beams based on moment-curvature relation," *Comput. Struc.*, vol. 80, pp. 615–628, Dec. 2002, http://dx.doi.org/10.12989/cac.2007.4.6.457.

[43] G. Kaklauskas and V. Gribniak, "Eliminating shrinkage effect from moment curvature and tension stiffening relationships of reinforced concrete members," *J. Struct. Eng.*, vol. 137, no. 12, pp. 1460–1469, Feb. 2011, http://dx.doi.org/10.1061/(asce)st.1943-541x.0000395.

[44] I. F. Kara, A. F. Ashour, and M. A. Koroglu, "Flexural behavior of hybrid FRP/steel reinforced concrete beams," *Compos. Struct.*, vol. 129, pp. 111–121, Oct. 2015, http://dx.doi.org/10.1016/j.compstruct.2015.03.073.

Author contributions: IRIP: conceptualization, methodology, investigation, writing - original draft. JJM: conceptualization, methodology, writing - original draft. CAB: Conceptualization, Writing - original draft. LCA: writing - review & editing, supervision, project administration, funding acquisition. LMT: writing - review & editing, supervision, project administration, funding acquisition. PAK: writing - review & editing.

Editors: Osvaldo Manzoli, Guilherme Aris Parsekian.